






Topological excitations and bound photon pairs in a superconducting quantum metamaterial

Ilya S. Besedin ^{1,2} Maxim A. Gorlach ³ Nikolay N. Abramov,^{1,2} Ivan Tsitsilin ^{1,2,4,*} Ilya N. Moskalenko ^{1,2}
Alina A. Dobronosova,^{5,6} Dmitry O. Moskalev,^{5,6} Alexey R. Matanin,^{5,6} Nikita S. Smirnov,^{5,6} Ilya A. Rodionov ^{5,6}
Alexander N. Poddubny,^{3,7,8} and Alexey V. Ustinov^{1,2,9}

¹*National University of Science and Technology MISIS, Moscow 119049, Russia*

²*Russian Quantum Center, Skolkovo, Moscow 143025, Russia*

³*School of Physics and Engineering, ITMO University, Saint Petersburg 197101, Russia*

⁴*Moscow Institute of Physics and Technology, Dolgoprudny 141700, Russia*

⁵*FMN Laboratory, Bauman Moscow State Technical University, Moscow 105005, Russia*

⁶*Dukhov Automatics Research Institute (VNIIA), Moscow 127055, Russia*

⁷*Ioffe Institute, Saint Petersburg 194021, Russia*

⁸*Nonlinear Physics Centre, Australian National University, Canberra ACT 2601, Australia*

⁹*Physikalisches Institut, Karlsruhe Institute of Technology, Karlsruhe 76131, Germany*



(Received 23 March 2021; accepted 1 June 2021; published 17 June 2021)

Recent discoveries in topological physics hold promise for disorder-robust quantum systems and technologies. Topological states provide the crucial ingredient of such systems featuring increased robustness to disorder and imperfections. Here we use an array of superconducting qubits to engineer a one-dimensional topologically non-trivial quantum metamaterial. By performing microwave spectroscopy of the fabricated array, we experimentally observe the spectrum of elementary excitations. We reveal not only the single-photon topological states but also the bands of exotic bound photon pairs arising due to the inherent anharmonicity of qubits. Furthermore, we discuss the formation of the two-photon bound edge-localized state and confirm the topological origin of our model demonstrating disorder-robust behavior of photon-photon correlation function for the topological edge state. Our work provides an experimental implementation of the topological model with attractive photon-photon interaction in a quantum metamaterial.

DOI: [10.1103/PhysRevB.103.224520](https://doi.org/10.1103/PhysRevB.103.224520)

I. INTRODUCTION

Superconducting qubits are a viable platform for scalable quantum computers. Realization of quantum computation protocols and eventually quantum supremacy [1] relies largely on the coherent operation of ensembles of coupled qubits. A profound challenge in this direction is imposed by unavoidable parameter spread between the fabricated qubits of the ensemble. The need to control individual qubit parameters to reduce this spread makes scaling quantum computers up difficult.

Even less practical is the need of using individual qubit control tools for superconducting quantum metamaterials [2,3]—large arrays of interacting qubits, which can be viewed as an artificially created quantum matter. A promising way to tackle unavoidable irregularities in quantum metamaterials is provided by the concept of *topological states* whose existence is guaranteed by the global symmetries of the structure being insensitive to local imperfections [4,5]. Besides such remarkable features as disorder-robust propagation and localization of light [5], topological states hold promise for quantum technologies. In particular, recent studies suggest that a pair of photons propagating via topological mode preserves quantum

correlations significantly longer than a photon pair propagating in the bulk [6–8].

Photon-photon interactions arising due to the nonlinearity of the medium provide an exciting additional degree of freedom giving rise to a plethora of topological phenomena including interaction-induced topological states. One of the simplest interacting models is the paradigmatic Bose-Hubbard model, which arises in various contexts including cold atom ensembles in optical lattices [9], magnetic insulators [10], as well as arrays of transmon qubits. The inherent anharmonicity of transmon qubit potential enables strong photon-photon interactions [11]. Combining this feature with fine-tuning of qubit eigenfrequency or temporal modulation of qubit couplings, one can switch the system into the quantum Hall phase [12,13]. Note that the elementary bosonic excitations in qubit array are, strictly speaking, plasmon-polaritons as they are superpositions of plasma oscillations in Josephson junctions and distributed electric fields in their environment [14], and we term them “photons” only for the sake of simplicity.

An interesting feature of the Bose-Hubbard model is the emergence of bound boson pairs (doublons) mediated by the interactions [15,16]. Such quasiparticles can localize at the edge of the system forming a two-photon bound edge state, which arises even in the absence of single-photon localized states [17,18]. The topological physics of doublons has been extensively explored in a series of recent theoretical works [19–22] and also emulated with a classical system of higher

*Current address: Walther-Meißner-Institut, Bayerische Akademie der Wissenschaften, D-85748 Garching, Germany.

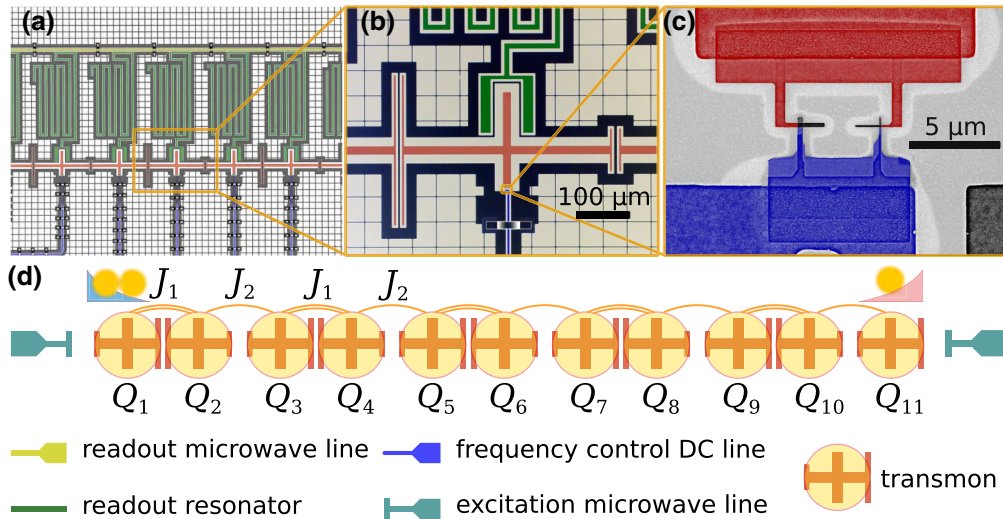


FIG. 1. Implementation of the Su-Schrieffer-Heeger model (SSH) with the array of transmon qubits. (a) False-color image of the array of transmon qubits. Each qubit (shown by red) is capacitively coupled to a resonator for readout (green) and a frequency control line (blue). The readout resonators are coupled to a feedline (yellow). To probe two possible terminations of the array simultaneously, we consider the structure consisting of $N = 11$ qubits. (b) Enlarged fragment showing the geometry of the individual transmon qubit. (c) False-color SEM image of transmon junctions. (d) The sketch of the designed structure showing the effective coupling amplitudes and the location of single-photon topological state and two-photon bound edge-localized state.

dimensionality [18]. However, the experimental investigation of topological properties of bound photon pairs is still lacking.

To fill this gap and to highlight the important aspects of topological protection in interacting quantum models, we design and investigate experimentally a dimerized array of qubits with alternating nearest-neighbor coupling strengths [Figs. 1(a)–1(c)]. This quantum metamaterial, depicted schematically in Fig. 1(d), provides a realization of the well-celebrated topologically nontrivial Su-Schrieffer-Heeger model (SSH) [23], which has been implemented in a variety of systems ranging from simple mechanical [24] or microwave [25] structures to photonic [26], polaritonic [27], and cold atom [28] realizations. Importantly, in contrast to the previous studies of one-dimensional topological qubit arrays [29,30], we probe here not only the single-photon excitations but also the two-photon ones, examining such exotic phenomena as bound photon pairs and their interaction-induced localization. Furthermore, we highlight the topological origin of our model calculating photon-photon correlation function $g^{(2)}(0)$ and demonstrating its robustness to disorder for the scenario of topological edge state excitation.

The rest of the article is organized as follows. Section II describes the studied system; Secs. III and IV outline the theoretical and experimental results for the single- and two-photon excitations in the fabricated array of qubits. We draw conclusions in Sec. V, while additional details on tight-binding calculations, sample fabrication, and measurement procedure appear as Appendixes A–C, respectively. Further details are provided in the supplemental material [31].

II. ARRAY OF QUBITS

The circuit that we studied consists of $N = 11$ nearest-neighbor coupled superconducting transmon qubits described

by the Bose-Hubbard Hamiltonian

$$\hat{\mathcal{H}}_{\text{BH}}/h = \sum_{q=1}^N \left[f_q \hat{n}_q + \frac{\delta_q}{2} \hat{n}_q (\hat{n}_q - 1) \right] + \sum_{q=1}^{(N-1)/2} [J_1 \hat{a}_{2q} \hat{a}_{2q-1}^\dagger + J_2 \hat{a}_{2q} \hat{a}_{2q+1}^\dagger] + \text{H.c.}, \quad (1)$$

where $\hat{n}_q = \hat{a}_q^\dagger \hat{a}_q$ is the photon number operator; f_q is the eigenfrequency of q th transmon, which can be flexibly tuned in the range from 3.73 to 3.82 GHz; $\delta_q = -155$ MHz is the qubit anharmonicity responsible for the effective photon-photon interaction; and the amplitudes $J_1 = 55.1$ MHz and $J_2 = 17.1$ MHz describe the nearest-neighbor coupling of qubits. All qubits are tuned to the same frequency equal to $f_0 = 3.8$ GHz and $f'_0 = 3.75$ GHz in the single-photon and two-photon experiments, respectively. To probe the modes of qubit array, we apply a monochromatic driving with frequency f_d and amplitude Ω . The design of the sample includes two excitation lines that allow excitation from either edge of the array, $s = 1$ or $s = 11$. To determine the time-averaged population of each site, we exploit a frequency-multiplexed readout scheme, which includes coplanar waveguide resonators dispersively coupled to each of the qubits, and a coplanar waveguide feedline. Further details on the sample design and on the retrieval of its parameters are provided in Secs. III and IV of Ref. [31].

In the absence of driving and dissipation, the Bose-Hubbard model conserves the number of photons which allows one to label all eigenstates by the associated photon number. Hence, in the driven-dissipative case, depending on the driving frequency and amplitude, one can address either the single-photon sector of the Hilbert space (at low power) or

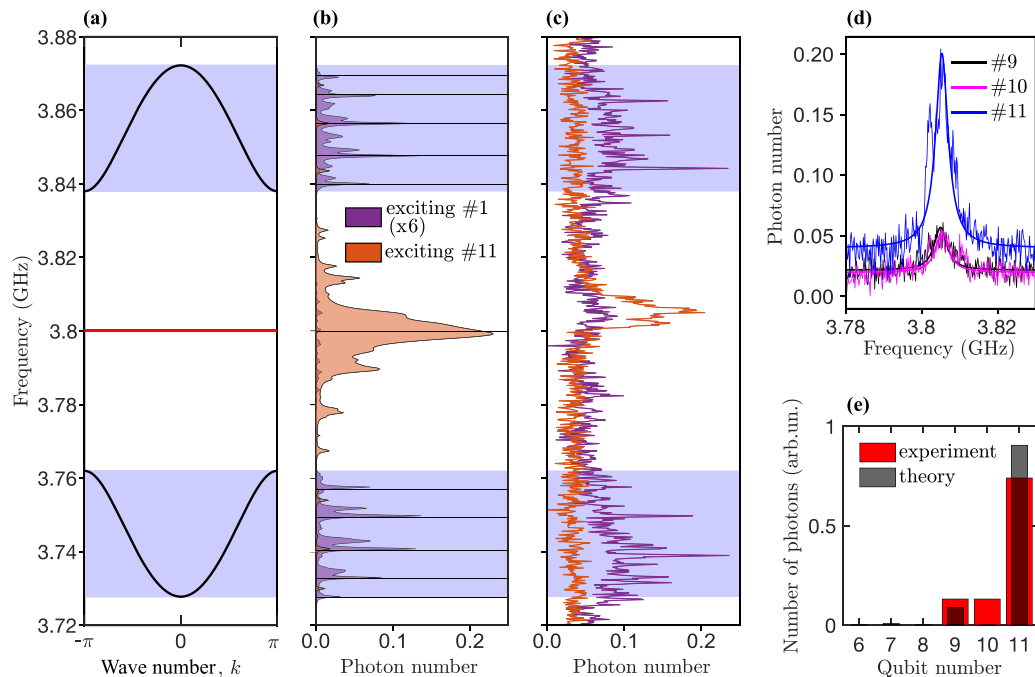


FIG. 2. Spectroscopy of single-photon excitations in qubit array. (a) Dispersion of single-photon excitations in the array of qubits tuned to the same frequency $f_0 = 3.8$ GHz. Shaded areas illustrate the boundaries of the bulk bands. The horizontal line at the frequency 3.8 GHz depicts the spectral position of the single-photon topological state. (b) Calculated spectra of the average number of photons versus driving frequency for excitation and readout of the first (magenta color) or last (red color) qubits of the array. Calculation details are provided in Sec. II of Ref. [31]. (c) Experimental spectra showing the dependence of normalized average photon number in the array versus driving frequency. Magenta and red colors correspond to the excitation and readout of the first and the last qubits in the array, respectively. (d) Average photon number measured in qubits Nos. 9, 10, and 11 versus driving frequency when qubit No. 11 is excited. (e) Single-photon probability distribution for the edge state extracted from the amplitudes of the peaks measured for qubits Nos. 9, 10, and 11 and depicted in (d).

the two-photon eigenstates (at higher power), which are manifested as characteristic peaks in measured photon number versus driving frequency. Anharmonicity of qubit potential δ_q gives rise to the frequency shift between the two types of states. An additional benchmark to experimentally distinguish these states is provided by the characteristic dependence of resonance linewidth on the driving power [Supplemental Fig. S4 of Ref. [31]].

III. SINGLE-PHOTON TOPOLOGICAL STATES

For the single-photon excitations, the interaction term $\propto \delta_q$ in the Hamiltonian Eq. (1) is not manifested, and the physics of this system is captured by the SSH model. Therefore, we expect two bands of single-photon states with the dispersion given by

$$f = f_0 \pm \sqrt{J_1^2 + J_2^2 + 2J_1 J_2 \cos k}, \quad (2)$$

as illustrated in Fig. 2(a). Here, the Bloch wave number k ranges from $-\pi$ to π taking quantized values in a finite system. As a result, exciting the system at the first qubit and measuring the expectation value of the photon number operator $\langle \hat{n}_1 \rangle$, we expect a series of distinct peaks corresponding to the bulk modes of the array [Fig. 2(b)] emergent in the experimental data [Fig. 2(c)].

Single-photon excitations described by Eq. (2) are spread over the entire array. However, besides such delocalized exci-

tations the system also supports an edge-localized topological state with the frequency precisely in the middle of bandgap, $f_{\text{edge}} = f_0$. The wave function of this state exhibits an exponential localization at the edge of the array with the weak tunneling link, i.e., at the 11th qubit. Therefore, exciting the array at the last qubit, we couple predominantly to the edge state manifested as a sharp peak in the middle of the bulk band gap [Fig. 2(b), red color]. A similar peak is observed in the experimental data [Fig. 2(c)] providing direct evidence of the single-photon edge state in the SSH-type array of coupled qubits. Note that the spectral positions of the peaks in the experimental data and in the simulation are slightly different due to the residual disorder in the qubit frequency after calibration as quantified in Sec. I and Sec. IV of Ref. [31].

Besides providing the spectroscopic evidence of a single-photon topological state, we also examine the probability distribution for the observed mode. To this end, we excite the array at the 11th qubit and measure the average photon occupancy in qubits Nos. 11, 10, and 9 versus driving frequency, as shown in Fig. 2(d). All three curves have a similar shape featuring a pronounced peak at the same frequency corresponding to the resonant excitation of the single-photon edge state. The amplitudes of these peaks are related to the eigenmode profile, which allows us to extract the probability distribution for the edge mode directly from the experimental data. The extracted results are compared with the predictions of the tight-binding model in the histogram in Fig. 2(e). As expected, the probability amplitude decays away from the

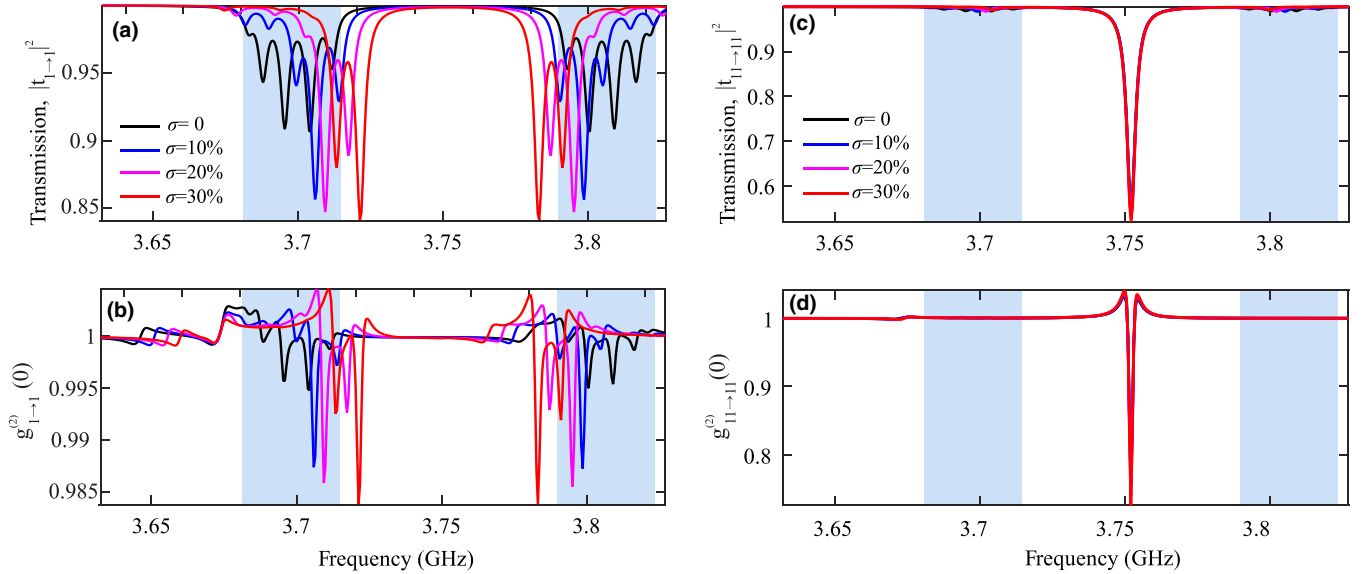


FIG. 3. Topological protection of edge state eigenfrequency and two-photon quantum correlations. (a) Calculated linear transmission coefficient for the array of 11 qubits tuned to resonance at 3.752 GHz with the alternating coupling constants $J_1 = 55.1$ MHz and $J_2 = 17.1$ MHz for the different levels of disorder σ in the coupling strengths. Shaded domains indicate the frequencies of bulk single-photon states. Anharmonicity of qubits $\delta = -155$ MHz. Radiative and nonradiative decay rates are taken to be $\Gamma_0 = 0.5$ MHz and $\Gamma = 1.5$ MHz, respectively. Excitation and detection are performed at qubit No. 1. (b) Calculated $g^{(2)}(0)$ correlation function for the same array. Excitation and detection are performed at qubit No. 1. (c, d) Calculated linear transmission coefficient (c) and $g^{(2)}(0)$ correlation function (d) for the same array. Excitation and detection are performed at qubit No. 11.

edge of the array, which clearly confirms the edge-localized nature of the observed single-photon state. Note, however, that the experimental data show nonzero photon population in qubit No. 10, contrary to the idealized theoretical model. Our numerical simulations (Ref. [31], Sec. VIII) suggest that this discrepancy arises due to the significant dephasing present in qubit No. 11 as well as other qubits of the array.

To reveal the features of topological protection in the designed structure, we simulate linear transmission coefficients and $g^{(2)}(0)$ correlation functions for our system versus excitation frequency employing the approach of Refs. [32–34] (the details of the calculations are provided in Sec. VII of Ref. [31]). First, we calculate the transmission coefficient $t_{1 \rightarrow 1}$ when excitation and detection are performed at the left edge of the array [Fig. 3(a)]. The characteristic dips in the transmission correspond to the bulk modes of the array. Increasing the disorder in the capacitive coupling of qubits, we observe spectral shifts of the dips growing with the strength of the disorder. The similar situation is observed for $g^{(2)}$ correlation function [Fig. 3(b)].

Next, we perform the same calculation for the scenario when driving and detection are performed at the right edge of the array (qubit No. 11) supporting the localized edge state. In such case, the edge state determines the response of the system giving rise to the pronounced dip in the middle of the bulk band gap [Fig. 3(c)]. Contrary to the results above, the spectral position of the dip as well as its amplitude feature the same behavior for all levels of disorder.

In a similar way, we assess $g^{(2)}$ correlation function in the presence of disorder. Similarly to the transmission coefficient, the spectrum of $g^{(2)}$ features a characteristic dip almost unaffected by disorder when the array is driven from the right

edge. Therefore, we conclude that the topological origin of our model enables the robustness of photonic $g^{(2)}$ correlation function which remains insensitive to the fluctuations in qubit capacitive couplings.

The observed behavior is a consequence of the chiral symmetry, which protects the frequency of the edge state against fluctuations in the coupling constants. It should be stressed, however, that the edge state is not robust against disorder in qubit eigenfrequencies, since the latter breaks chiral symmetry of the model shifting the frequency and distorting the profile of the edge mode.

IV. TWO-PHOTON BOUND STATES

The two-photon modes of the designed system feature more complex behavior than their single-photon counterparts and belong to four major types [19,35]. The majority of the two-photon eigenstates is presented by the scattering states with the energy given by the sum of single-photon energies in the continuum limit. The second group is the single-photon edge states, where one photon is localized at the weak link edge of the array, whereas the second photon propagates along the array (see details in Sec. VI of Ref. [31]). These two types of modes strongly resemble those in the single-particle SSH model.

However, the effects of interaction give rise to two novel types of modes associated with bound photon pairs (doublons) as well as their edge states. The bulk spectrum of the system features four doublon bands [19,35]. Two doublon bands have the frequency which scales linearly with δ being detuned from the scattering continuum approximately by $\delta = -155$ MHz. The dispersion of these two doublon bands calculated by the

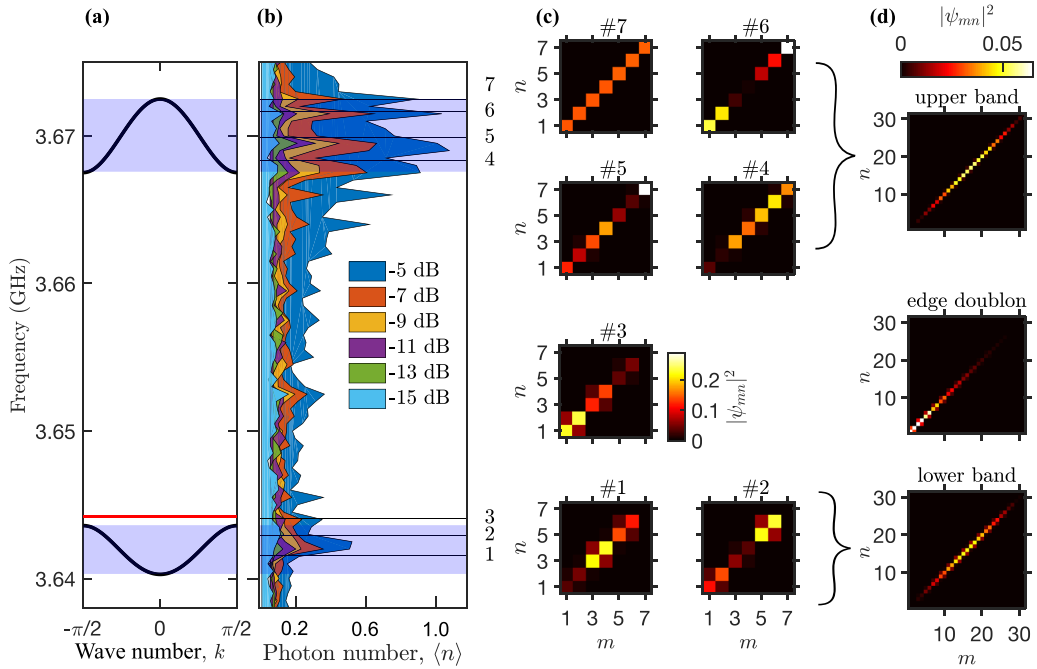


FIG. 4. Spectroscopy of two-photon excitations in qubit array. (a) Calculated dispersion of bound photon pairs in a periodic array. Higher-frequency two-photon scattering states are not shown. The red horizontal line shows the spectral position of the doublon edge state localized at the opposite edge of the semi-infinite array compared to the single-photon state. (b) Experimental spectrum of normalized average photon number in the array when excitation and readout are applied at the first qubit. Shaded areas show the boundaries of bulk doublon bands. In this experiment, the array consists of 7 qubits tuned to resonance at 3.75 GHz. The driving powers from -15 dB to -5 dB correspond to the amplitudes of the drive equal to 1.3, 1.7, 2.1, 2.7, 3.4, and 4.3 MHz. (c) The calculated two-photon probability distributions for the array of 7 qubits. The numbers near each panel correspond to the characteristic peaks marked in panel (b). Panel #3 shows the signatures of interaction-induced edge localization which can be demonstrated more clearly for longer arrays. (d) Calculated two-photon probability distribution in the array of 31 qubit for the three representative cases: upper doublon band (top), doublon edge state (middle), and lower doublon band (bottom).

modified Bethe ansatz method [19] is presented in Fig. 4(a). While bulk doublon dispersion strongly resembles that of the SSH model, the doublon edge state obtained in our calculations [Fig. 4(a)] exhibits quite unexpected features. Contrary to the single-photon scenario, it is localized at the strong link edge of the array, providing an example of interaction-induced localization.

Due to the good spectral isolation of the discussed doublon bands, the respective two-photon states can be probed spectroscopically. For that purpose, we apply the driving signal to the first qubit of the array measuring the spectrum of photon number amplitudes $\langle \hat{n}_1 \rangle$ [Fig. 4(b)]. While at low input powers we do not observe any pronounced features in the spectrum, the situation changes significantly when input power is increased up to the level allowing two-photon transitions in qubits. In agreement with the calculated positions of bulk doublon bands, two separate groups of peaks emerge.

To visualize the eigenstates underlying those peaks, we calculate the associated two-photon probability distributions shown in Fig. 4(c). It is clearly seen that all 7 eigenstates correspond to bound photon pairs, since the two photons most likely share the same qubit. However, the length of the array is insufficient to discriminate between bulk and edge doublon states. To clarify this, we perform the numerical diagonalization of the Hamiltonian for a larger system composed of 31 qubit [Fig. 4(d)]. The upper group of peaks is related to

antisymmetric doublon states when the phase of the doublon wave function for the adjacent positions of bound photon pair differs by π , whereas the lower group is associated with symmetric doublon states when the respective phase difference is equal to 0. The doublon edge state emerges at the upper boundary of the lower band and features relatively weak interaction-induced localization with the localization length exceeding 10 sites.

Even though the localized state fully shows up for long arrays with $N \gtrsim 15$ qubits (see Ref. [31], Sec. V), we can identify the state #3 as a precursor of the edge-localized doublon state. This points toward interaction-induced localization in our system, which is especially pronounced for the arrays with odd N , in which case the doublon edge state arises only at a single edge.

V. CONCLUSIONS

To conclude, our experiments demonstrate the power of qubit arrays for exploring few-photon topological physics. As we prove, the topological nature of the model protects not only the frequency of the topological edge state but also the $g^{(2)}$ correlation function. At the same time, the two-photon spectrum is dramatically enriched compared to the noninteracting scenario. Interactions give rise to exotic bound photon pairs whose energies and wave functions can be probed spectroscopically. Furthermore, our system exhibits

the signatures of interaction-induced two-photon localization. This highlights a promise of interacting models for quantum topological photonics, paving a way toward disorder-robust quantum metamaterials.

ACKNOWLEDGMENTS

The authors acknowledge valuable discussions with Andrei Stepanenko. Development of theoretical models was supported by the Russian Foundation for Basic Research (Grant No. 18-29-20037). Russian Science Foundation supported the experiments (Contract No. 16-12-00095) and numerical simulations (Contract No. 20-72-10065). M.A.G. acknowledges partial support by the Foundation for the Advancement of Theoretical Physics and Mathematics “Basis.” A.V.U. acknowledges partial support by the Deutsche Forschungsgemeinschaft (DFG) by the Grant No. US 18/15-1. Sample studied in this work was made at the BMSTU Nanofabrication Facility (FMN Laboratory, FMNS REC, ID 74300). The MISIS team acknowledges support from the Ministry of Education and Science of the Russian Federation in the framework of the Increase Competitiveness Program of the Ministry of Education and Science of the Russian Federation MISIS (Contract No. K2-2020-017). The RQC team acknowledges the support of this work by Rosatom.

APPENDIX A: TIGHT BINDING SIMULATIONS

To find the eigenstates of the Bose-Hubbard Hamiltonian Eq. (1), we use the fact that the Hamiltonian $\hat{\mathcal{H}}_{\text{BH}}$ commutes with the operator $\hat{n} = \sum_q \hat{n}_q$. This means that the total number of photons in this model is conserved, and the two-photon wave function can be presented in the form

$$|\psi\rangle = \frac{1}{\sqrt{2}} \sum_{m,n} \beta_{mn} \hat{a}_m^\dagger \hat{a}_n^\dagger |0\rangle, \quad (\text{A1})$$

where $\beta_{mn} = \beta_{nm}$ are the unknown superposition coefficients. The two-photon eigenstates are found from the Schrödinger equation $\hat{\mathcal{H}}_{\text{BH}} |\psi\rangle = \varepsilon |\psi\rangle$. Combining Eqs. (1) and (A1), we obtain the linear system of equations for the unknown superposition coefficients:

$$(\varepsilon - \delta) \beta_{mn} = -2J_{n-1} \beta_{n-1,n} - 2J_n \beta_{n,n+1}, \quad (\text{A2})$$

$$\begin{aligned} \varepsilon \beta_{mn} = & -J_{m-1} \beta_{m-1,n} - J_{n-1} \beta_{m,n-1} \\ & - J_m \beta_{m+1,n} - J_n \beta_{m,n+1}, \end{aligned} \quad (\text{A3})$$

where $m < n$, $\beta_{0n} = 0$, $J_n = J_1$ for odd n and $J_n = J_2$ for even n . Solving this system numerically, we find the two-photon eigenstates supported by the finite array. The frequencies shown in Figs. 2–4 correspond to $\varepsilon/(2\hbar)$.

APPENDIX B: SAMPLE FABRICATION

The sample is made in a three-stage process: (I) Base Al layer patterning, (II) Josephson junction double-angle evaporation and lift-off, and (III) low impedance crossover fabrication to suppress stray microwave chip modes. We use a high-resistivity intrinsic silicon substrate ($\rho > 10000 \Omega \cdot \text{cm}$, $500 \mu\text{m}$ thick) prepared by Piranha-based wet cleaning and

HF dip to remove surface oxide damage. The qubit capacitors, ground plane, readout resonators, and control wiring are made using e-beam evaporated 100-nm-thick epitaxial Al [36] and subsequent patterning by means of direct laser lithography and BCl_3/Cl_2 inductively coupled plasma etch. The native Al oxide is removed with *in situ* Ar-ion milling, followed by Al-AlOx-Al Josephson junction e-beam shadow evaporation ($\pm 11^\circ$, 25/45 nm) and lift-off in N-methyl-2-pyrrolidone at 80°C . Finally, low impedance free-standing crossovers are fabricated in a process similar to the fabrication steps outlined in Ref. [37], with an important improvement: we have used Al dry etching (Cl_2 -based) to pattern crossovers instead of wet process and redesign crossover topology to eliminate the Al base layer damage and provide mA-range crossover critical current.

APPENDIX C: MEASUREMENT SCHEME

We perform continuous wave two-tone spectroscopy by measuring the shift of the scattering amplitude at the frequency of the unperturbed readout resonator $\Delta S_{21}(f_r)$ while applying a monochromatic drive tone with amplitude Ω and frequency f_d . The drive tone is applied to one of the edges of the array. The readout circuitry of the sample is designed such that the scattering amplitude shift is proportional to the energy stored in the corresponding transmon.

The first condition for this regime of operation is that all dispersive shifts χ are at least order of magnitude less than the resonator linewidths, yielding the first-order expansion

$$\langle \Delta S_{21}(f_r) \rangle = \frac{\partial S_{21}^{\text{notch}}(f, f_r, Q_l, Q_c)}{\partial f_r} \chi_q \langle n \rangle, \quad (\text{C1})$$

where $S_{21}^{\text{notch}}(f, f_r, Q_l, Q_c)$ is the theoretical frequency dependence of the S_{21} parameter for resonator frequency f_r , its loaded and external quality factors Q_l and Q_c , respectively [38], and $\langle n \rangle$ is the mean number of photons in transmon.

The second condition requires that the anharmonicity of the transmons is order of magnitude less than the qubit-transmon detuning

$$|\delta_q| \ll |f_r - f_q|.$$

To the first order in δ and second order in the qubit-resonator coupling constant g , the dispersive shift is given by

$$\chi_q = -\frac{2g^2 \delta_q}{(f_r - f_q)^2}. \quad (\text{C2})$$

For the single-photon state measurements, we convert the scattering amplitude shift into mean photon number, computing the coefficient from Eqs. (C1) and (C2).

The bare frequencies of the qubits are set to their target values using individual DC flux control lines, each coupled to one of the qubits. Mutual inductances between the flux lines and SQUIDs of the corresponding qubit, as well as its nearest neighbors, frozen-in flux values, precise values of Josephson junction critical currents, and qubit-resonator coupling have been extracted from fitting a series of two-tone calibration measurements to a linear oscillator model (see Ref. [31], Sec. IV). The values of J_1, J_2 and δ are determined from electrostatic simulation.

The measurements at $f = 3.8$ GHz have been performed with a frequency resolution 0.2 MHz with a Rabi drive amplitude $\Omega/2\pi = 0.30$ MHz. At the same time, power-sweep measurements at $f' = 3.75$ GHz have been carried out with 0.5 MHz frequency resolution.

Note that the features of the spectrum that are not related to the external drive, such as quasithermal residual transmon population, cannot be determined from $\langle n \rangle$ in such spectra. Other manifestations of quasithermal effects are discussed in Sec. I of Ref. [31].

-
- [1] F. Arute, K. Arya, R. Babbush, D. Bacon, J. C. Bardin, R. Barends, R. Biswas, S. Boixo, F. G. S. L. Brandao *et al.*, Quantum supremacy using a programmable superconducting processor, *Nature* **574**, 505 (2019).
- [2] P. Macha, G. Oelsner, J. M. Reiner, M. Marthaler, S. André, G. Schön, U. Hübner, H. G. Meyer, E. Il'ichev, and A. V. Ustinov, Implementation of a quantum metamaterial using superconducting qubits, *Nat. Commun.* **5**, 5146 (2014).
- [3] P. Jung, A. V. Ustinov, and S. M. Anlage, Progress in superconducting metamaterials, *Supercond. Sci. Tech.* **27**, 073001 (2014).
- [4] L. Lu, J. D. Joannopoulos, and M. Soljačić, Topological photonics, *Nat. Photon.* **8**, 821 (2014).
- [5] T. Ozawa, H. M. Price, A. Amo, N. Goldman, M. Hafezi, L. Lu, M. C. Rechtsman, D. Schuster, J. Simon, O. Zilberberg, and I. Carusotto, Topological photonics, *Rev. Mod. Phys.* **91**, 015006 (2019).
- [6] A. Blanco-Redondo, B. Bell, D. Oren, B. J. Eggleton, and M. Segev, Topological protection of biphoton states, *Science* **362**, 568 (2018).
- [7] Y. Wang, X.-L. Pang, Y.-H. Lu, J. Gao, Y.-J. Chang, L.-F. Qiao, Z.-Q. Jiao, H. Tang, and X.-M. Jin, Topological protection of two-photon quantum correlation on a photonic chip, *Optica* **6**, 955 (2019).
- [8] M. Wang, C. Doyle, B. Bell, M. J. Collins, E. Magi, B. J. Eggleton, M. Segev, and A. Blanco-Redondo, Topologically protected entangled photonic states, *Nanophotonics* **8**, 1327 (2019).
- [9] D. Jaksch and P. Zoller, The cold atom Hubbard toolbox, *Ann. Phys.* **315**, 52 (2005).
- [10] T. Giamarchi, C. Rüegg, and O. Tchernyshyov, Bose-Einstein condensation in magnetic insulators, *Nat. Phys.* **4**, 198 (2008).
- [11] I. Carusotto, A. A. Houck, A. J. Kollár, P. Roushan, D. I. Schuster, and J. Simon, Photonic materials in circuit quantum electrodynamics, *Nat. Phys.* **16**, 268 (2020).
- [12] P. Roushan, C. Neill, A. Megrant, Y. Chen, R. Babbush, R. Barends, B. Campbell, Z. Chen, B. Chiaro, A. Dunsworth *et al.*, Chiral ground-state currents of interacting photons in a synthetic magnetic field, *Nat. Phys.* **13**, 146 (2017).
- [13] P. Roushan, C. Neill, J. Tangpanitanon, V. M. Bastidas, A. Megrant, R. Barends, Y. Chen, Z. Chen, B. Chiaro, A. Dunsworth *et al.*, Spectroscopic signatures of localization with interacting photons in superconducting qubits, *Science* **358**, 1175 (2017).
- [14] M. Leib and M. Hartmann, Bose-Hubbard dynamics of polaritons in a chain of circuit quantum electrodynamics cavities, *New J. Phys.* **12**, 093031 (2010).
- [15] D. C. Mattis, The few-body problem on a lattice, *Rev. Mod. Phys.* **58**, 361 (1986).
- [16] K. Winkler, G. Thalhammer, F. Lang, R. Grimm, J. H. Denschlag, A. J. Daley, A. Kantian, H. P. Büchler, and P. Zoller, Repulsively bound atom pairs in an optical lattice, *Nature* **441**, 853 (2006).
- [17] M. A. Gorlach and A. N. Poddubny, Interaction-induced two-photon edge states in an extended Hubbard model realized in a cavity array, *Phys. Rev. A* **95**, 033831 (2017).
- [18] N. A. Olekhno, E. I. Kretov, A. A. Stepanenko, P. A. Ivanova, V. V. Yaroshenko, E. M. Puhtina, D. S. Filonov, B. Cappello, L. Matekovits, and M. A. Gorlach, Topological edge states of interacting photon pairs emulated in a topoelectrical circuit, *Nat. Commun.* **11**, 1436 (2020).
- [19] M. A. Gorlach and A. N. Poddubny, Topological edge states of bound photon pairs, *Phys. Rev. A* **95**, 053866 (2017).
- [20] G. Salerno, M. Di Liberto, C. Menotti, and I. Carusotto, Topological two-body bound states in the interacting Haldane model, *Phys. Rev. A* **97**, 013637 (2018).
- [21] G. Salerno, G. Palumbo, N. Goldman, and M. Di Liberto, Interaction-induced lattices for bound states: Designing flat bands, quantized pumps, and higher-order topological insulators for doublons, *Phys. Rev. Research* **2**, 013348 (2020).
- [22] A. A. Stepanenko and M. A. Gorlach, Interaction-induced topological states of photon pairs, *Phys. Rev. A* **102**, 013510 (2020).
- [23] A. J. Heeger, S. Kivelson, J. R. Schrieffer, and W. P. Su, Solitons in conducting polymers, *Rev. Mod. Phys.* **60**, 781 (1988).
- [24] C. L. Kane and T. C. Lubensky, Topological boundary modes in isostatic lattices, *Nat. Phys.* **10**, 39 (2014).
- [25] A. P. Slobozhanyuk, A. N. Poddubny, A. E. Miroshnichenko, P. A. Belov, and Y. S. Kivshar, Subwavelength Topological Edge States in Optically Resonant Dielectric Structures, *Phys. Rev. Lett.* **114**, 123901 (2015).
- [26] N. Malkova, I. Hromada, X. Wang, G. Bryant, and Z. Chen, Observation of optical Shockley-like surface states in photonic superlattices, *Opt. Lett.* **34**, 1633 (2009).
- [27] P. St-Jean, V. Goblot, E. Galopin, A. Lemaître, T. Ozawa, L. L. Gratiet, I. Sagnes, J. Bloch, and A. Amo, Lasing in topological edge states of a one-dimensional lattice, *Nat. Photonics* **11**, 651 (2017).
- [28] S. de Léséleuc, V. Lienhard, P. Scholl, D. Barredo, S. Weber, N. Lang, H. P. Büchler, T. Lahaye, and A. Browaeys, Observation of a symmetry-protected topological phase of interacting bosons with Rydberg atoms, *Science* **365**, 775 (2019).
- [29] W. Cai, J. Han, F. Mei, Y. Xu, Y. Ma, X. Li, H. Wang, Y. P. Song, Z.-Y. Xue, Z. QiYin, S. Jia, and L. Sun, Observation of Topological Magnon Insulator States in a Superconducting Circuit, *Phys. Rev. Lett.* **123**, 080501 (2019).
- [30] E. Kim, X. Zhang, V. S. Ferreira, J. Banker, J. K. Iverson, A. Sipahigil, M. Bello, A. González-Tudela, M. Mirhosseini, and O. Painter, Quantum Electrodynamics in a Topological Waveguide, *Phys. Rev. X* **11**, 011015 (2021).
- [31] See Supplemental Material at <http://link.aps.org/supplemental/10.1103/PhysRevB.103.224520> for details on theoretical analysis and experimental investigation of the fabricated qubit array.

- [32] Y.-L. L. Fang, H. Zheng, and H. U. Baranger, One-dimensional waveguide coupled to multiple qubits: photon-photon correlations, *EPJ Quantum Technol.* **1**, 3 (2014).
- [33] A. V. Poshakinskiy and A. N. Poddubny, Biexciton-mediated superradiant photon blockade, *Phys. Rev. A* **93**, 033856 (2016).
- [34] Y. Ke, A. V. Poshakinskiy, C. Lee, Y. S. Kivshar, and A. N. Poddubny, Inelastic Scattering of Photon Pairs in Qubit Arrays with Subradiant States, *Phys. Rev. Lett.* **123**, 253601 (2019).
- [35] M. Di Liberto, A. Recati, I. Carusotto, and C. Menotti, Two-body physics in the Su-Schrieffer-Heeger model, *Phys. Rev. A* **94**, 062704 (2016).
- [36] I. A. Rodionov, A. S. Baburin, A. R. Gabidullin, S. S. Maklakov, S. Peters, I. A. Ryzhikov, and A. V. Andriyash, Quantum engineering of atomically smooth single-crystalline silver films, *Sci. Rep.* **9**, 12232 (2019).
- [37] Z. Chen, A. Megrant, J. Kelly, R. Barends, J. Bochmann, Y. Chen, B. Chiaro, A. Dunsworth, E. Jeffrey, J. Y. Mutus, P. J. O'Malley, C. Neill, P. Roushan, D. Sank, A. Vainsencher, J. Wenner, T. C. White, A. N. Cleland, and J. M. Martinis, Fabrication and characterization of aluminum airbridges for superconducting microwave circuits, *Appl. Phys. Lett.* **104**, 052602 (2014).
- [38] S. Probst, F. B. Song, P. A. Bushev, A. V. Ustinov, and M. Weides, Efficient and robust analysis of complex scattering data under noise in microwave resonators, *Rev. Sci. Instrum.* **86**, 024706 (2015).